Peroxiredoxin 4 suppresses ferroptosis in esophageal squamous cell carcinoma by activating the phosphoinositide 3-kinase signaling pathway

KE LI[1*], SHUNING XU[1*], HONGTAO LIU[2], TIANLI FAN[3], YIYANG LI[2], RUILI REN[2], YUE XU[4], SHENGLEI LI[4] and YING LIU[1]

[1]Department of Oncology, The Affiliated Cancer Hospital of Zhengzhou University and Henan Cancer Hospital, Zhengzhou, Henan 450008, P.R. China; [2]School of Life Sciences, Zhengzhou University, Zhengzhou, Henan 450001, P.R. China; [3]Department of Pharmacology, School of Basic Medicine, Zhengzhou University, Zhengzhou, Henan 450001, P.R. China; [4]Department of Pathology, The First Affiliated Hospital of Zhengzhou University, Zhengzhou, Henan 450052, P.R. China

Received October 16, 2025; Accepted February 20, 2026

DOI: 10.3892/br.2026.2133

Abstract. Peroxiredoxin 4 (PRDX4) has been found to be upregulated and verified to play protective roles against oxidative stress in various tumors. However, its exact function and underlying molecular mechanisms in esophageal squamous cell carcinoma (ESCC) remain unclear. The aim of the present study was to evaluate the roles of PRDX4 in ferroptosis of ESCC cells and elucidate its potential molecular mechanisms. Bioinformatics analysis, western blotting and reverse transcription-quantitative PCR confirmed that PRDX4 was markedly upregulated in ESCC samples and cells. The close association of PRDX4 with lymph node metastasis and TNM staging was identified, and PRDX4 may be an independent prognostic marker for patients with ESCC. Furthermore, PRDX4 depletion inhibited the proliferation and invasion of ESCC cells, whereas PRDX4 overexpression had the opposite effect. Notably, PRDX4 knockdown promoted ferroptosis by increasing malondialdehyde and lipid peroxidation levels, and decreasing glutathione levels, coupled with decreased expression of glutathione peroxidase 4 and solute carrier family 7 member 11, and increased expression of prostaglandin-endoperoxide synthase 2. However, PRDX4 overexpression showed opposite effects, which were partly reversed by the ferroptosis inhibitor, ferrostatin-1 and the inducer erastin. Most crucially, PRDX4 depletion-mediated inactivation of the phosphoinositide 3-kinase (PI3K)/AKT signaling pathway could be rescued by 740 Y-P (a PI3K activator), whereas PRDX4 overexpression triggered the activation of the PI3K/AKT signaling pathway, which could be reversed by the PI3K inhibitor LY294002. Collectively, the data suggest that PRXD4 suppresses ferroptosis in ESCC cells by activating the PI3K/AKT signaling pathway, suggesting that targeting PRDX4 may be a novel strategy for treating patients with ESCC.

Correspondence to: Dr Ying Liu, Department of Oncology, The Affiliated Cancer Hospital of Zhengzhou University and Henan Cancer Hospital, 127 Dongming Road, Zhengzhou, Henan 450008, P.R. China
E-mail: liuying20031022@126.com

*Contributed equally

Key words: peroxiredoxin 4, esophageal squamous cell carcinoma, ferroptosis, lipid peroxidation, PI3K/AKT signaling pathway, prognosis

Introduction

Esophageal cancer (ESCA) is one of the most frequently diagnosed tumors of the digestive system worldwide, ranking seventh in incidence and sixth in mortality (1). Esophageal squamous cell carcinoma (ESCC), the main histological subtype of ESCA, is prevalent in developing countries such as the Middle East and East Asia, particularly in China (2,3). Although numerous clinical trials have greatly improved the therapeutic efficacy of ESCC, the 5-year survival rate of patients with ESCC is ~20% (4). In addition, the lack of effective diagnostic and therapeutic biomarkers results in poor prognosis for patients with ESCC (5). Therefore, it is imperative to identify novel molecular markers to improve the prognosis and therapeutic efficacy in patients with ESCC.

Peroxiredoxins (PRDXs) constitute a family of peroxidase enzymes (PRDX1-6) characterized by a catalytic cysteine residue embedded within the evolutionarily conserved motif PXXXTXXC (6-8). From a functional perspective, the six mammalian peroxiredoxins (PRDX1-6) exhibit distinct characteristics in terms of subcellular localization, susceptibility to hyperoxidation, substrate specificity, and the presence or absence of an additional resolving cysteine residue (9,10). Several studies have demonstrated that PRDX4, a major factor of redox balance, shields cells from reactive oxygen species (ROS)-induced oxidative damage by diminishing peroxides, such as hydrogen peroxide (H_2O_2) (11,12). Elevated ROS levels have been implicated in the pathological and physiological

processes of a broad range of diseases, such as cancer and neurodegenerative disorders (13,14). In addition, tumor cells often experience oxidative stress due to increased ROS levels (15), which in turn results in damaged biomacromolecules (lipids, proteins, and DNA), thus triggering strong cell toxicity (16). Wang *et al* (17) found that PRDX4 knockdown elicited ROS overproduction in hepatocellular carcinoma (17). PRDX4 has been widely reported to participate in the development and progression of various tumors, such as breast cancer (18), hepatoblastoma (19), renal cell carcinoma (20), uterine corpus endometrial carcinoma (21), pancreatic ductal adenocarcinoma (22), and gastric cancer (23). Moreover, PRDX4 has been developed as a biomarker and a novel therapeutic target for renal papillary cell carcinoma and pancreatic cancer (24). These studies suggest that targeting PRDX4 may be an attractive therapeutic strategy for a variety of tumors. However, whether PRDX4-mediated tumor-promoting effects make it an attractive target for patients with ESCC remains to be investigated.

Ferroptosis, firstly discovered in 2012 is a type of iron-dependent regulated cell death caused by excessive lipid peroxidation (25), and is different from other programmed cell death processes, including apoptosis, necrosis, and pyroptosis (26). Numerous antioxidants and other related factors, such as glutathione peroxidase 4 (GPX4), ferroptosis suppressor protein 1, and dihydroorotate dehydrogenase, have been shown to inhibit ferroptosis (27-29). Several studies have revealed the versatile functions of ferroptosis in numerous tumors, including cell growth, metastasis, immune surveillance, and therapeutic response (30-33). Recent studies have focused on the relationship between PRDX proteins and ferroptosis. For example, genetic ablation or knockdown of PRDX6 was shown to sensitize lung endothelial cells to erastin-induced ferroptosis (34). In addition, loss of PRDX6 downregulated selenoprotein expression and induced ferroptosis through GPX4 suppression (35). A previous study revealed that PRDX4 knockdown markedly promotes ROS production and induces ferroptosis in hepatic fibrosis (36). These studies indicate a strong association between PRDX and ferroptosis and suggest that targeting ferroptosis may be an emerging novel therapeutic strategy for patients with ESCC. However, whether PRDX4 participates in the regulation of ferroptosis and its precise molecular mechanisms in ESCC remain unclear.

The aim of the present study was to investigate the role of PRDX4 in ESCC and its underlying mechanism. PRDX4 expression was analyzed in clinical ESCC samples and cell lines, and its association with clinicopathological features was assessed. PRDX4 knockdown and overexpression models were used to evaluate its effects on cell proliferation, invasion, and ferroptosis. The involvement of the PI3K/AKT signaling pathway was examined to elucidate the molecular mechanism.

Materials and methods

Bioinformatics analysis. PRDX4 expression and pan-cancer prognostic values were analyzed using the Sangerbox 3.0 online database (http://vip.sangerbox.com/home.html). PRDX4 expression in ESCA and its association with patient survival was investigated using the UALCAN online database (http://ualcan.path.uab.edu/). The effect of PRDX4 on the overall survival of patients with ESCA was analyzed using the online databases, UALCAN and GEPIA (http://gepia.cancer-pku.cn/). GSE111011 was downloaded from the GEO database (https://www.ncbi.nlm.nih.gov/geo/query/acc.cgi?acc=GSE111011) for PRDX4 expression assay.

ESCC samples, cell lines, and cell cultures. A total of 65 ESCC samples along with paired normal samples were procured from the First Affiliated Hospital of Zhengzhou University (Zhengzhou, China). Patients with ESCC who had not received chemotherapy or radiotherapy were selected and provided written informed consent. Among the aforementioned cases, there were 39 males and 26 females, with a median age of 61 years (age range, 25-83 years). The experiments were approved (approval no. ZZUIRB 2023-239) by the Research and Ethics Committee of Zhengzhou University (Zhengzhou, China). The human ESCC cell line KYSE30 was purchased from Procell Life Science &Technology Co., Ltd. Normal esophageal epithelial cell line Het-1A and human ESCC cell lines KYSE520, KYSE70, KYSE450, and KYSE270, which were authenticated by STR profiling, were purchased from Qingqi Shanghai Biotechnology Development Co., Ltd. ESCC cells were cultured in RPMI-1640 medium (Procell Life Science & Technology Co., Ltd.) supplemented with 10% fetal bovine serum (FBS; Suzhou ShuangRu Biotech Co., Ltd.), as well as penicillin (100 U/ml) and streptomycin (0.1 mg/ml) solution (Solarbio Life Sciences), and were incubated at 37˚C with 5% CO_2.

Transfection of siRNA and plasmid. ESCC cells (KYSE30 and KYSE270) were plated in 6-well plates at $2x10^5$ cells per well and cultured in a CO_2 incubator for 24 h. When the cell confluency reached ~80%, 1.5 μg empty pcDNA3.1 vector and 1.5 μg PRDX4 overexpression vector, pcDNA3.1-PRDX4, were used to transfect into KYSE30 cells using Lipo8000™ Transfection Reagent (cat. no. C0533; Beyotime Institute of Biotechnology) according to manufacturer's protocol for 48 h at 37˚C. The old medium was replaced with fresh medium 6 h after transfection. The transfected cells were then incubated for an additional 48 h at 37˚C before being harvested for further analyses. In addition, a control siRNA (50 nM; cat. no. sc-37007; Santa Cruz Biotechnology, Inc.) and PRDX4 siRNA (50 nM; cat. no. sc-40835; Santa Cruz Biotechnology, Inc.) were transfected into KYSE270 cells using Lipo8000™ Transfection Reagent according to the manufacturer's instructions for 48 h at 37˚C. The old medium was replaced with fresh medium 6 h after transfection. The transfected cells were then incubated for an additional 48 h at 37˚C before being harvested for further analyses. Both the control siRNA and PRDX4 siRNA were commercially purchased from Santa Cruz Biotechnology, Inc. as validated, ready-to-use reagents with demonstrated high knockdown efficiency; however, the manufacturer's product documentation did not disclose the specific siRNA sequences.

Cell Counting Kit-8 (CCK-8) assay. A CCK-8 kit (cat. C0038; Beyotime, China) was used to assess cell proliferation. In brief, KYSE30 and KYSE270 cells with different transfection efficiencies (3,000 cells per well) were plated in a 96-well plate. Cell viability was measured at 24, 48, 72 and 96 h post-seeding by adding 10 μl of CCK-8 reagent to each well,

followed by incubation for 2 h at 37˚C. The absorbance value at 450 nm was determined at 24, 48, 72 and 96 h using a microplate reader.

Colony formation assay. A colony formation assay was performed to evaluate the colony formation ability of KYSE30 and KYSE270 cells. Briefly, transfected ESCC cells were plated in 6-well plates at a density of $1x10^3$ cells per well. The culture medium was replaced with fresh medium, and the cells were cultured for 9-12 days. Finally, the cells were fixed with 4% paraformaldehyde (cat. no. P1110; Solarbio Life Sciences) for 20 min at room temperature and stained with 0.1% crystal violet (cat. no. IC0600; Solarbio Life Sciences) for 30 min at room temperature. Colonies containing >50 cells were counted using ImageJ 1.8.0 software (NIH).

EdU staining. EdU staining was performed to detect the proliferative abilities of the ESCC cells. Briefly, transfected KYSE30 and KYSE270 cells were plated in 48-well plates at $5x10^3$ cells per well for 48 h. EdU (1:1,000 dilution; cat. no. C10310-1; Guangzhou RiboBio Co., Ltd.) was added to each well and incubated for 2 h at 37˚C. The cells were then fixed with 4% paraformaldehyde for 30 min at room temperature. Subsequently, glycine solution was added to each well for 5 min, and the penetrant reagent was added to each well for another 10 min. Next, 1X Apollo® staining solution (included in kit cat. no. C10310-1; Guangzhou RiboBio Co., Ltd.) was added to each well for 30 min at room temperature. Finally, ESCC cells were treated with Hoechst (1:100 dilution; included in kit cat. no. C10310-1; Guangzhou RiboBio Co., Ltd.) for 30 min at room temperature. Fluorescence images were acquired using an inverted fluorescence microscope, and at least five random fields of view were captured per well. EdU-positive cells were quantified using ImageJ 1.8.0 software [National Institutes of Health (NIH)].

Cell migration. A 24-well Transwell chamber (8-μm pores; Corning, Inc.) was used to examine the cell migration ability. Transfected KYSE30 and KYSE270 cells ($5x10^3$) cultured in 200 μl of FBS-free medium were seeded into a Matrigel-uncoated upper chamber (Transwell chamber, Corning, Inc.), and the lower chamber was filled with 600 μl of medium containing 20% FBS. Cells were maintained at 37˚C in a 5% CO_2 incubator for 48 h, fixed using 4% paraformaldehyde for 30 min at room temperature, stained with 0.1% crystal violet for 30 min at room temperature, and washed with PBS. Images were captured using an optical microscope.

Cell invasion. Cell invasion was investigated using a 24-well Transwell chamber with Matrigel (BD Biosciences, Inc.), and Matrigel-coated inserts were thawed and rehydrated with serum-free medium for 1 h at 37˚C prior to cell seeding. Transfected KYSE30 and KYSE270 cells ($5x10^3$) in serum-free medium were added to the top chamber of each well, and 600 μl complete medium supplemented with 20% FBS was applied to the lower chamber. The cells were incubated at 37˚C in a 5% CO_2 incubator for 48 h. Subsequently, the invasive cells were fixed using methanol for 30 min at room temperature, and stained with crystal violet for 30 min at room temperature. The stained invasive cells were counted using an optical microscope.

Analysis of malondialdehyde (MDA), lipid peroxidation (LPO) and glutathione (GSH) levels. KYSE30 and KYSE270 cells ($1x10^6$) were harvested 48 h after transfection and seeded into 6-well plates. The cells were then treated with erastin (5 μM), ferrostatin-1 (Fer-1; 10 μM), 740 Y-P (20 μM) and LY294002 (20 μM) (all from TargetMol Chemicals Corporation) for 24 h at 37˚C. Lipid peroxidation indicators were measured according to the manufacturer's protocol. MDA levels were detected using an MDA Content Detection kit (cat. no. S0131S; Beyotime Institute of Biotechnology), LPO levels were determined using an LPO Content Assay kit (cat. no. BC5245; Solarbio Life Sciences), and the GSH levels were measured using a GSH Detection kit (cat. no. BC1175; Solarbio Life Sciences).

Reverse transcription-quantitative PCR (RT-qPCR). Total RNA was extracted using TRIzol reagent (Solarbio Life Sciences), and transcribed into cDNA using the Prime-Script RT kit (Takara Bio, Inc.). cDNA was then added to the reaction system for PCR amplification using the SYBR Green PCR Master Mix (Takara Bio, Inc.). Subsequently, RT-qPCR was performed in 384-well plates using the real-time PCR system, LightCycler® 480 (Roche Diagnostics) according to the manufacturer's protocol. The following primers were used: PRDX4 (NM_006406, product size: 171 bp) forward, 5'-CGAAGA TTTCCAAGCCAGCG-3' and reverse, 5'-CAAGTCTGTCGC CAAAAGCG-3'; β-actin (NM_001101, produce size: 192 bp) forward: 5'-AACTGGGACGACATGGAGAAAA-3' and reverse, 5'-GGATAGCACAGCCTGGATAGCA-3'. β-actin was used as the control. Finally, the relative level of PRDX4 was analyzed from three independent experiments using the $2^{-\Delta\Delta Cq}$ method (37).

Western blotting. Total protein was extracted using RIPA lysis buffer (Solarbio Life Sciences). Protein concentration was determined using a BCA Protein Assay kit (Solarbio Life Sciences). Total proteins (50 μg) from each group were separated using 10% SDS-PAGE and transferred onto PVDF membranes (MilliporeSigma). After blocking with 5% skimmed milk, PVDF membranes were incubated with primary antibodies at 4˚C overnight. The primary antibodies were as follows: Anti-PRDX4 (1:2,000 dilution; cat. no. 10703-1-AP), anti-E-cadherin (1:20,000 dilution; cat. no. 20874-1-AP), anti-N-cadherin (1:2,000 dilution; cat. no. 22018-1-AP), anti-Vimentin (1:20,000 dilution; cat. no. 10366-1-AP), and anti-GPX4 (1:1,000 dilution; cat. no. 30388-1-AP; all from Proteintech Group, Inc.), anti-solute carrier family 7 member 11 (SLC7A11; 1:1,000 dilution; cat. no. DF12509; Affinity Biosciences, Ltd.), anti-prostaglandin-endoperoxide synthase 2 (PTGS2; 1:1,000 dilution; cat. no. 27308-1-AP; Proteintech Group, Inc.), anti-p-PI3K (1:1,000 dilution; cat. no. AP0427; ABclonal Biotech Co., Ltd.), anti-PI3K (1:1,000 dilution; cat. no. A19742; ABclonal Biotech Co., Ltd.), anti-p-AKT (1:2,000 dilution; cat. no. 28731-1-AP; Proteintech Group, Inc.), anti-AKT (1:2,000 dilution; cat. no. 10176-2-AP; Proteintech Group, Inc.) and anti-β-actin (1:2,000 dilution; cat. no. 20536-1-AP; Proteintech Group, Inc.). After washing with

Tris-buffered saline (TBS) with 0.05% Tween 20, the PVDF membranes were incubated with horseradish peroxidase (HRP)-labeled secondary antibody (1:10,000 dilution; cat. no. RGAR001; Proteintech Group, Inc.) for 2 h at 37˚C, and then rinsed with TBST. Subsequently, the PVDF membranes were incubated with chemiluminescent HRP substrate (Affinity Biosciences, Ltd.). Finally, the relative protein levels were analyzed using the ImageJ 1.8.0 software (NIH).

Immunohistochemistry (IHC). The tissue sections were fixed with 10% formalin for 24 h at room temperature, embedded in paraffin, and continuously cut into 4-6 μm sections. After dewaxing, rehydration, and antigen retrieval in citrate buffer (pH 6.0) using microwave heating and blocking with 10% goat serum (cat. no. C0265; Beyotime Insitute of Biotechnology) for 1 h at room temperature, tissue sections were incubated with anti-PRDX4 (1:2,000 dilution; cat. no. 10703-1-AP; Proteintech Group, Inc.) overnight at 4˚C. After washing, the corresponding HRP-labeled secondary antibody (1:5,000; cat. no. RGAR001; Proteintech Group, Inc.) were added to the tissue slides. The DAB reagent was used to generate the staining signals. The images were obtained using an optical microscope.

Statistical analysis. All experimental data are expressed as the mean ± SD, and were analyzed using GraphPad Prism software (version 8.0) for statistical assay. All experiments were independently repeated at least three times with distinct biological samples. Prior to parametric analyses, a normality distribution test was conducted to assess the data. Student's t-test or Mann-Whitney U test were utilized to compare two groups, and Differences among three or more groups were assessed by one-way ANOVA followed by Tukey's HSD post hoc test. $P<0.05$ was considered to indicate a statistically significant difference.

Results

PRDX4 is highly expressed in ESCA. PRDX4 expression was investigated in ESCA using TCGA database. PRDX4 was highly expressed in all the investigated tumor types, with low expression in pancreatic adenocarcinoma (PAAD) and kidney chromophobe (KICH) tumors (Fig. 1A). Data from the UALCAN database revealed that the expression of PRDX4 in ESCA samples was significantly higher than that in normal samples (Fig. 1B), which was also validated by GEO dataset GSE111011 (Fig. 1C). In addition, RT-qPCR revealed that the mRNA levels of PRDX4 in 65 ESCC samples were significantly higher than those in the paired normal samples (Fig. 1D). Furthermore, the expression of PRDX4 was examined in eight ESCC samples and paired normal samples by western blotting and it was found that the expression of PRDX4 in all ESCC samples was higher than that in paired normal samples (Fig. 1E and F), which was also verified by IHC assay (Fig. 1G). Further investigation revealed that PRDX4 expression in a panel of ESCC cell lines was significantly higher than that in the normal esophageal epithelial cell line Het-1A (Fig. 1H-J). These findings indicated that PRDX4 was highly expressed in ESCC tissues and cells.

High PRDX4 expression as a potential prognostic marker in ESCC. To further dissect the clinical value of PRDX4 in ESCC, TCGA database was used to investigate the expression of PRDX4 on the survival rate of patients with ESCA. Patients with high PRDX4 expression had lower survival rates than those with low PRDX4 expression (Fig. 2A and B). Moreover, high PRDX4 expression predicted a poor prognosis in patients with ESCA (Fig. 2C). Further investigation revealed that high PRDX4 expression was closely associated with TNM staging and lymph node metastasis (Fig. 2D and E). Notably, patients with ESCC with high PRDX4 expression had lower survival rates than those with low PRDX4 expression (Fig. 2F). These findings indicated that PRDX4 is involved in ESCC progression and may serve as a novel prognostic marker for patients with this disease.

PRDX4 knockdown suppresses cell proliferation in ESCC cells. To further explore the biological role of PRDX4 in ESCC, ESCC cells were transfected with PRDX4 siRNA and the overexpression vector pcDNA3.1-PRDX4. PRDX4 siRNA significantly downregulated PRDX4 expression in KYSE520 cells with high PRDX4 expression (Fig. 3A and B), whereas pcDNA3.1-PRDX4 markedly upregulated PRDX4 expression in KYSE30 cells with low PRDX4 expression (Fig. 3A and B), which was further validated using RT-qPCR (Fig. 3C). Further investigation indicated that PRDX4 depletion inhibited cell proliferation and colony formation (Fig. 3D-F), whereas PRDX4 overexpression had the opposite effects (Fig. 3G-I). Furthermore, EdU staining revealed that PRDX4 downregulation markedly reduced the number of EdU-positive cells, whereas PRDX4 overexpression markedly increased the number of EdU-positive cells (Fig. 3J-M). These findings indicated that PRDX4 functions as an oncogene in ESCC cells.

PRDX4 depletion inhibits cell migration and invasion in ESCC cells. In the present study, the role of PRDX4 in ESCC cell migration and invasion was explored. The results revealed that PRDX4 downregulation markedly suppressed ESCC cell migration and invasion (Fig. 4A-C). Western blot analysis demonstrated that PRDX4 knockdown markedly promoted the expression of E-cadherin, but reduced the expression of N-cadherin and vimentin (Fig. 4D and E). Conversely, PRDX4 overexpression significantly increased the migration and invasion abilities of ESCC cells (Fig. 4F-H), reduced E-cadherin expression, and increased N-cadherin and vimentin expression (Fig. 4I and J). These findings indicated that PRDX4 is an important regulator of ESCC cell invasion.

PRDX4 knockdown promotes ferroptosis in ESCC cells. Considering the important role of PRDX4 in oxidative stress, it was investigated whether PRDX4 affected ferroptosis in ESCC cells. It was revealed that PRDX4 depletion increased the levels of MDA and LPO but reduced the levels of GSH in ESCC cells (Fig. 5A). Furthermore, western blotting revealed that PRDX4 knockdown reduced the expression of ferroptosis inhibitory factors, such as GPX4 and SLC7A11, but increased the levels of the ferroptosis-promoting factor, PTGS2 (Fig. 5B and C). By contrast, PRDX4 overexpression significantly reduced the levels of MDA and LPO, but increased the levels of GSH in ESCC cells (Fig. 5D),

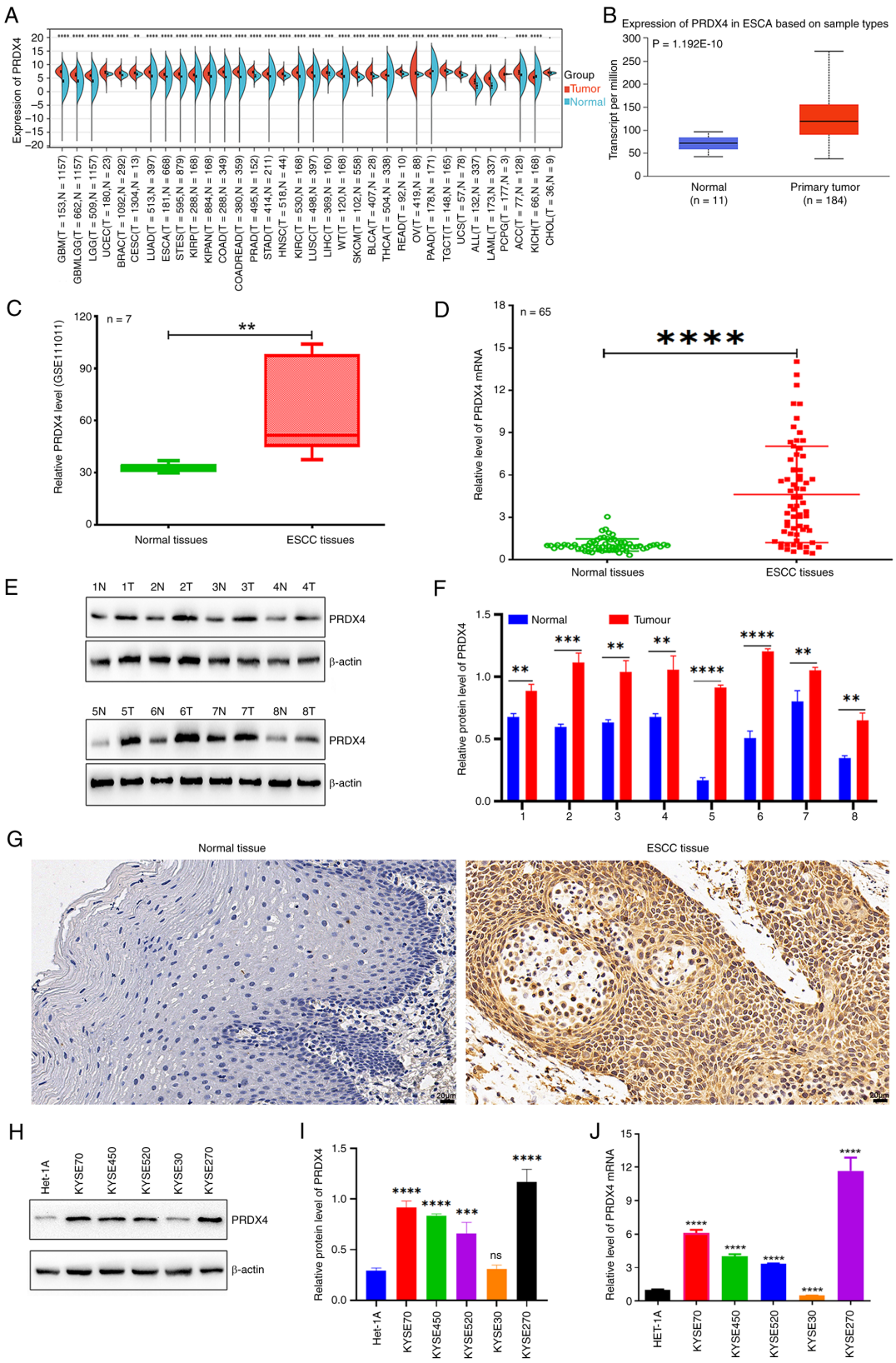

Figure 1. PRDX4 exhibits high expression in ESCC tissues and cells. (A) Sangerbox 3.0 online software assay for PRDX4 expression in pan-cancer. (B) UALCAN database investigation for PRDX4 expression in ESCA samples and normal esophageal epithelial tissues. (C) GEO dataset GSE111011 was used to investigate the expression of PRDX4 in ESCC samples and paired normal samples. (D) RT-qPCR assay was used to assess the expression of PRDX4 in 65 ESCC samples and paired normal samples. (E) Western blot analysis of the protein expression of PRDX4 in eight ESCC samples and paired normal samples. (F) The relative protein levels of PRDX4 in eight ESCC samples and paired normal samples. (G) IHC detection of PRDX4 expression in normal tissues and ESCC tissues. Scale bar, 20 μm. (H) Western blot analysis of PRDX4 protein expression in ESCC cell lines (KYSE70, KYSE450, KYSE520, KYSE30 and KYSE270) and normal esophageal epithelial cell line Het-1A. (I) The relative protein levels of PRDX4 in ESCC cell lines and Het-1A cells. (J) RT-qPCR assay of PRDX4 mRNA expression in the aforementioned ESCC cell lines and Het-1A cells. **P<0.01, ***P<0.001 and ****P<0.0001, indicate statistical significance. PRDX4, peroxiredoxin 4; ESCC, esophageal squamous cell carcinoma; ESCA, esophageal carcinoma; RT-qPCR, reverse transcription-quantitative polymerase chain reaction; GEO, Gene Expression Omnibus; IHC, immunohistochemistry; ns, not significant.

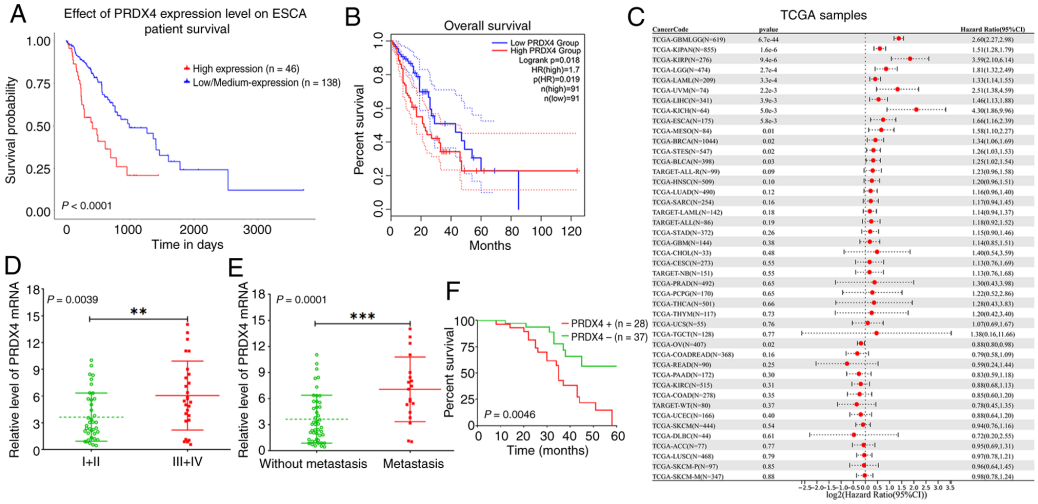

Figure 2. High expression of PRDX4 predicts a poor prognosis in patients with ESCC (A) UALCAN assay of the effects of PRDX4 expression on the survival of patients with ESCA. (B) GEPIA online software assay of the effects of PRDX4 expression on the survival of patients with ESCA. (C) Sangerbox 3.0 online software assay identifying high PRDX4 expression as a poor prognostic factor in patients with ESCA. (D) RT-qPCR assay for PRDX4 expression in patients with ESCC with different TNM stages. (E) RT-qPCR assay of PRDX4 expression in patients with ESCC without lymph node metastasis and with lymph node metastasis. (F) Log-rank test determination of the prognostic value of PRDX4 in patients with ESCC. **P<0.01 and ***P<0.001, indicate statistical significance. PRDX4, peroxiredoxin 4; ESCC, esophageal squamous cell carcinoma; ESCA, esophageal carcinoma; GEPIA, Gene Expression Profiling Interactive Analysis; RT-qPCR, reverse transcription quantitative polymerase chain reaction; TNM, tumor-node-metastasis.

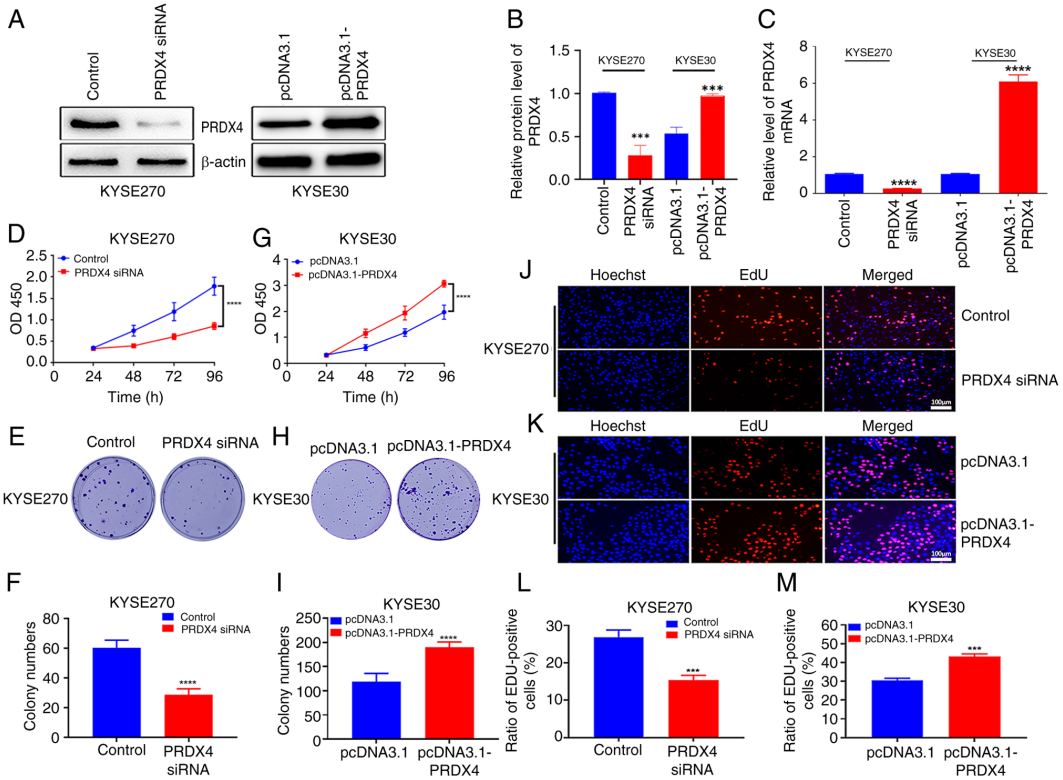

Figure 3. PRDX4 knockdown suppresses cell proliferation in ESCC cells. (A) Western blot analysis of the protein expression of PRDX4 in KYSE270 cells transfected with PRDX4 siRNA and KYSE30 cells transfected with pcDNA3.1-PRDX4. (B) The relative protein levels of PRDX4 in KYSE270 and KYSE30 cells with different transfections. (C) RT-qPCR assay of the mRNA expression of PRDX4 in KYSE270 cells transfected with PRDX4 siRNA and KYSE30 cells transfected with pcDNA3.1-PRDX4. (D) CCK-8 assay of cell proliferation in KYSE270 cells transfected with PRDX4 siRNA. (E) Colony formation assay of the colony-forming ability of KYSE270 cells transfected with PRDX4 siRNA. (F) Statistical analysis of the number of colonies formed in KYSE270 cells transfected with PRDX4 siRNA. (G) CCK-8 assay of cell proliferation in KYSE30 cells transfected with pcDNA3.1-PRDX4. (H) Colony formation assay of the colony-forming ability of KYSE30 cells transfected with pcDNA3.1-PRDX4. (I) Statistical analysis of the number of colonies formed in KYSE30 cells transfected with pcDNA3.1-PRDX4. (J) EdU staining assay of EdU-positive cells in KYSE270 cells transfected with PRDX4 siRNA. Scale bar, 100 μm. (K) EdU staining assay of EdU-positive cells in KYSE30 cells transfected with pcDNA3.1-PRDX4. Scale bar, 100 μm. (L) Statistical analysis of the number of EdU-positive cells in KYSE270 cells transfected with PRDX4 siRNA. (M) Statistical analysis of the number of EdU-positive cells in KYSE30 cells transfected with pcDNA3.1-PRDX4. ***P<0.001 and ****P<0.0001, indicate statistical significance. PRDX4, peroxiredoxin 4; ESCC, esophageal squamous cell carcinoma; siRNA, small interfering RNA; RT-qPCR, reverse transcription-quantitative polymerase chain reaction; CCK-8, Cell Counting Kit-8; EdU, 5-ethynyl-2'-deoxyuridine.

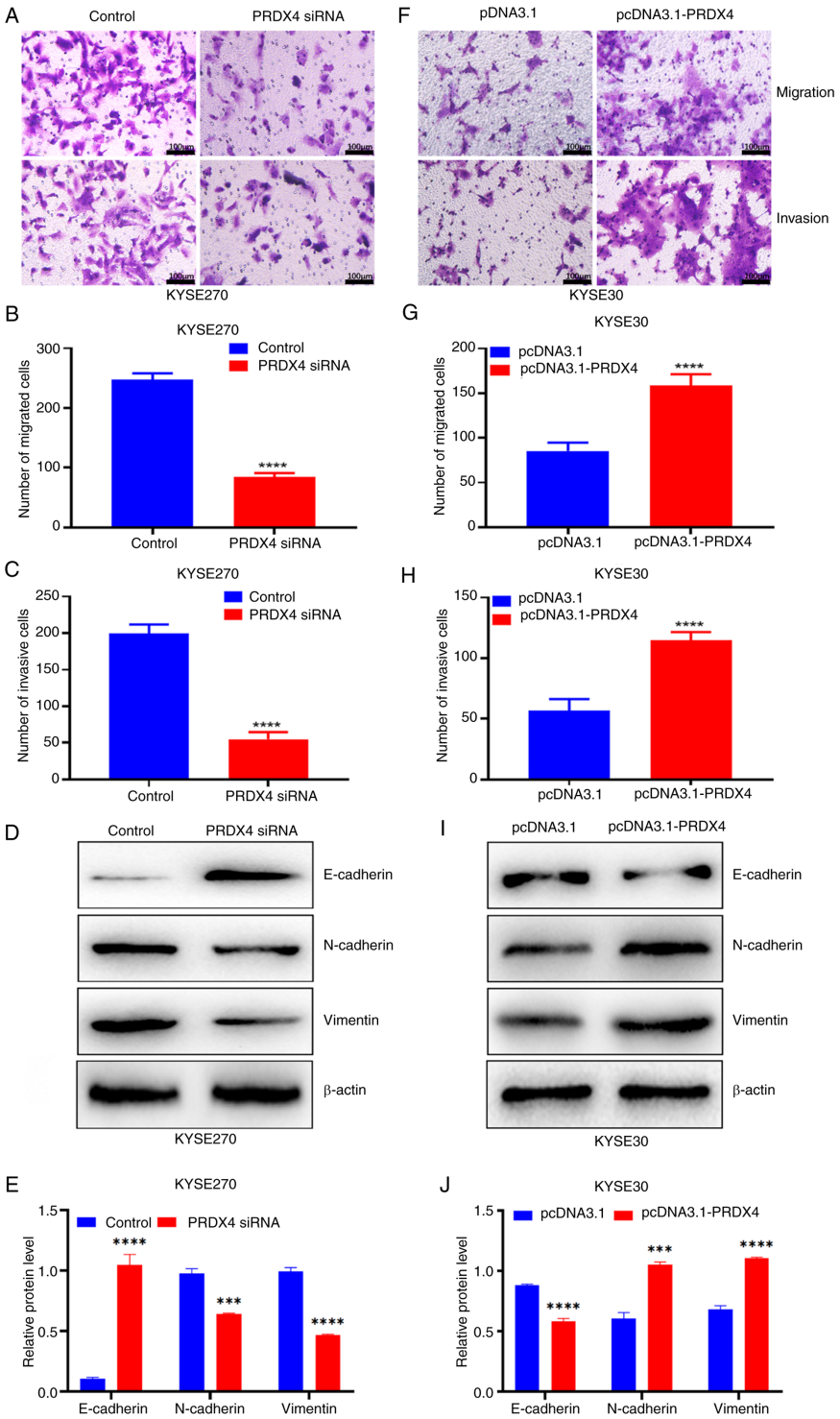

Figure 4. PRDX4 downregulation suppresses cell migration and invasion in ESCC cells. (A) PRDX4 knockdown suppresses cell migration and invasion in KYSE270 cells after transfection with PRDX4 siRNA. Scale bar, 100 μm. (B) Statistical analysis of the number of migratory cells in KYSE270 cells transfected with PRDX4 siRNA. (C) Statistical analysis of the number of invasive cells in KYSE270 cells transfected with PRDX4 siRNA. (D) Western blot analysis of the expression levels of E-cadherin, N-cadherin and vimentin in KYSE270 cells transfected with PRDX4 siRNA. (E) The relative protein levels of E-cadherin, N-cadherin and vimentin in KYSE270 cells transfected with PRDX4 siRNA. (F) PRDX4 overexpression suppresses cell migration and invasion in KYSE30 cells after transfection with pcDNA3.1-PRDX4. Scale bar, 100 μm. (G) Statistical analysis of the number of migratory cells in KYSE30 cells transfected with pcDNA3.1-PRDX4. (H) Statistical analysis of the number of invasive cells in KYSE30 cells transfected with pcDNA3.1-PRDX4. (I) Western blot analysis of the expression levels of E-cadherin, N-cadherin and vimentin in KYSE30 cells transfected with pcDNA3.1-PRDX4. (J) The relative protein levels of E-cadherin, N-cadherin and vimentin in KYSE30 cells transfected with pcDNA3.1-PRDX4. ***P<0.001 and ****P<0.0001, indicate statistical significance. PRDX4, peroxiredoxin 4; ESCC, esophageal squamous cell carcinoma; siRNA, small interfering RNA.

accompanied by enhanced GPX4 and SLC7A11 levels and decreased PTGS2 levels (Fig. 5E and F). Notably, Fer-1 partly reversed the changes in the levels of MDA, LPO, and GSH, as well as the expression of GPX4, SLC7A11, and PTGS2 proteins induced by PRDX4 siRNA in KYSE270 cells (Fig. 5G-I). Similarly, erastin effectively induced

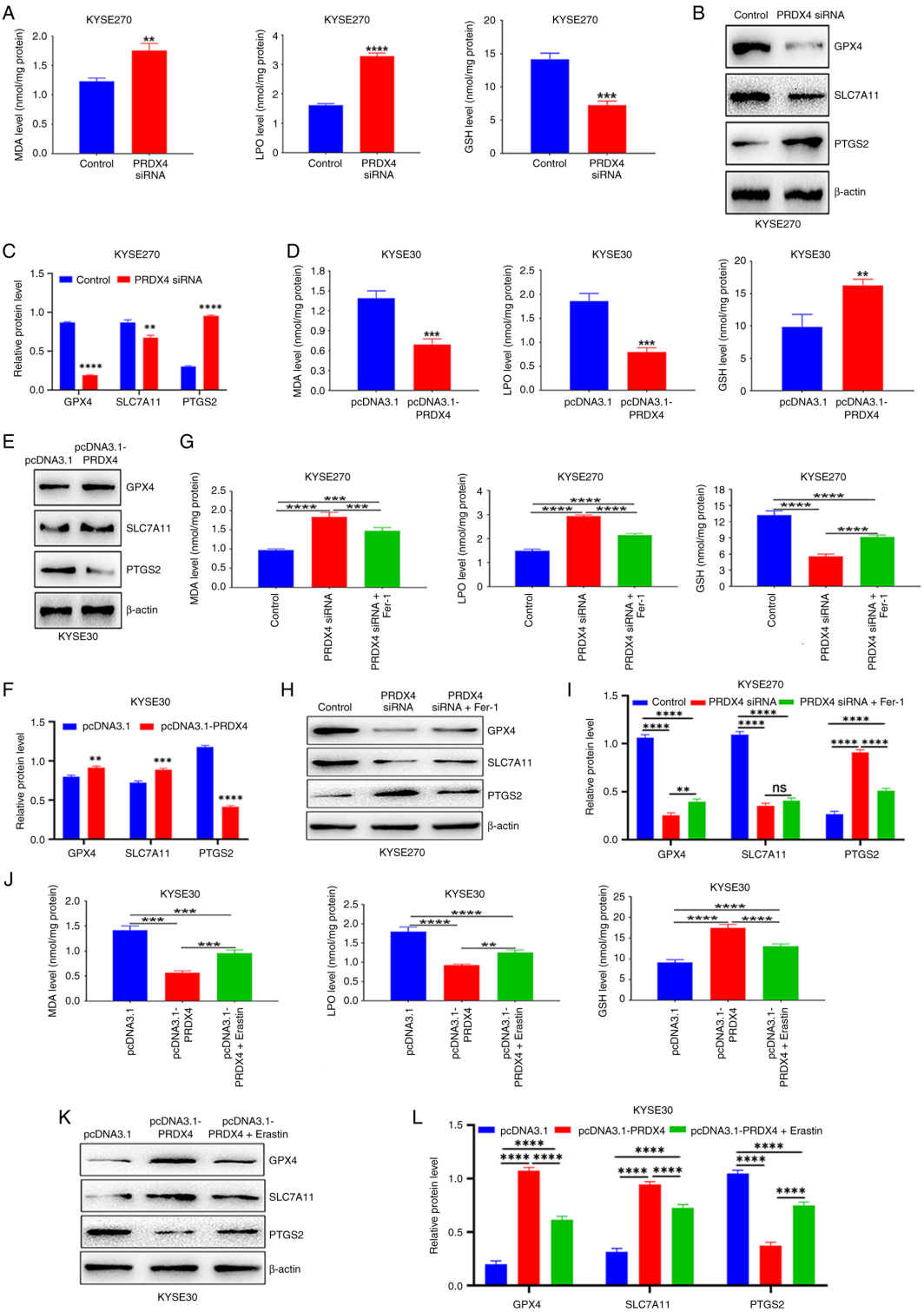

Figrue 5. PRDX4 is an important regulator of ferroptosis in ESCC cells. (A) Determination of MDA, LPO and GSH contents in KYSE270 cells after transfection with PRDX4 siRNA. (B) Western blot analysis of the protein levels of GPX4, SLC7A11 and PTGS2 in KYSE270 cells transfected with PRDX4 siRNA. (C) The relative protein levels of GPX4, SLC7A11 and PTGS2 in KYSE270 cells transfected with PRDX4 siRNA. (D) Determination of MDA, LPO and GSH contents in KYSE30 cells after transfection with pcDNA3.1-PRDX4. (E) Western blot analysis of the protein levels of GPX4, SLC7A11 and PTGS2 in KYSE30 cells transfected with pcDNA3.1-PRDX4. (F) The relative protein levels of GPX4, SLC7A11 and PTGS2 in KYSE30 cells transfected with pcDNA3.1-PRDX4. (G) Detection of the levels of MDA, LPO and GSH in the control group, PRDX4 siRNA group and PRDX4 siRNA plus Fer-1 group in KYSE270 cells. (H) Western blot analysis of the protein expression levels of GPX4, SLC7A11 and PTGS2 in the control group, PRDX4 siRNA group and PRDX4 siRNA plus Fer-1 group in KYSE270 cells. (I) The relative protein levels of GPX4, SLC7A11 and PTGS2 in the control group, PRDX4 siRNA group and PRDX4 siRNA plus Fer-1 group in KYSE270 cells. (J) Detection of the levels of MDA, LPO and GSH in the pcDNA3.1 group, pcDNA3.1-PRDX4 group and pcDNA3.1-PRDX4 plus erastin group in KYSE30 cells. (K) Western blot analysis of the protein expression levels of GPX4, SLC7A11 and PTGS2 in the pcDNA3.1 group, pcDNA3.1-PRDX4 group and pcDNA3.1-PRDX4 plus erastin group in KYSE30 cells. (L) The relative protein levels of GPX4, SLC7A11 and PTGS2 in the pcDNA3.1 group, pcDNA3.1-PRDX4 group and pcDNA3.1-PRDX4 plus erastin group in KYSE30 cells. **P<0.01, ***P<0.001 and ****P<0.0001, indicate statistical significance. PRDX4, peroxiredoxin 4; ESCC, esophageal squamous cell carcinoma; siRNA, small interfering RNA; MDA, malondialdehyde; LPO, lipid peroxidation; GSH, glutathione; GPX4, glutathione peroxidase 4; SLC7A11, solute carrier family 7 member 11; PTGS2, prostaglandin-endoperoxide synthase 2; Fer-1, ferrostatin-1; ns, not significant.

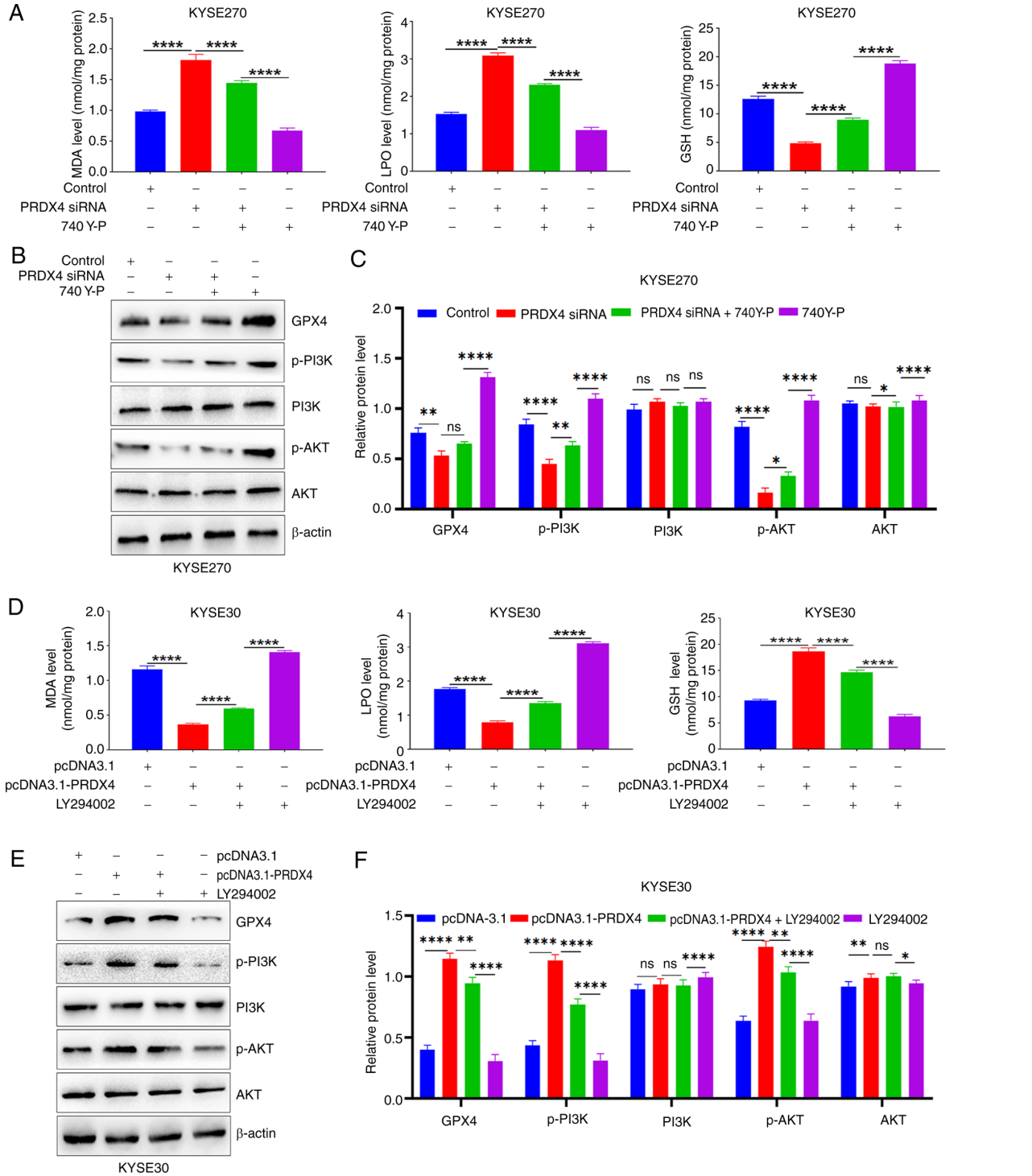

Figure 6. PRDX4 suppresses ferroptosis of ESCC cells by activating the PI3K/AKT signaling pathway. (A) Determination of MDA, LPO and GSH contents in the absence or presence of the PI3K activator 740 Y-P after PRDX4 knockdown in KYSE270 cells. (B) Western blot analysis of the protein expression levels of GPX4, p-PI3K, PI3K, p-AKT and AKT in the absence or presence of the PI3K activator 740 Y-P after PRDX4 knockdown in KYSE270 cells. (C) The relative protein levels of GPX4, p-PI3K, PI3K, p-AKT and AKT in the absence or presence of the PI3K activator 740 Y-P after PRDX4 knockdown in KYSE270 cells. (D) Detection of MDA, LPO and GSH contents in the absence or presence of the PI3K inhibitor LY294002 after PRDX4 overexpression in KYSE30 cells. (E) Western blot analysis of the protein expression levels of GPX4, p-PI3K, PI3K, p-AKT and AKT in the absence or presence of the PI3K inhibitor LY294002 after PRDX4 overexpression in KYSE30 cells. (F) The relative protein levels of GPX4, p-PI3K, PI3K, p-AKT and AKT in the absence or presence of the PI3K inhibitor LY294002 after PRDX4 overexpression in KYSE30 cells. *P<0.05, **P<0.01, and ****P<0.0001, indicate statistical significance. PRDX4, peroxiredoxin 4; ESCC, esophageal squamous cell carcinoma; PI3K, phosphoinositide 3-kinase; AKT, protein kinase B; MDA, malondialdehyde; LPO, lipid peroxidation; GSH, glutathione; GPX4, glutathione peroxidase 4; p-PI3K, phosphorylated PI3K; p-AKT, phosphorylated AKT; ns, not significant.

ferroptosis, which was suppressed by PRDX4 overexpression in KYSE30 cells, coupled with alterations in the levels of key ferroptosis-related proteins, such as GPX4, SLC7A11, and PTGS2 (Fig. 5J-L). These findings indicated that PRDX4 may participate in the regulation of ferroptosis in ESCC cells.

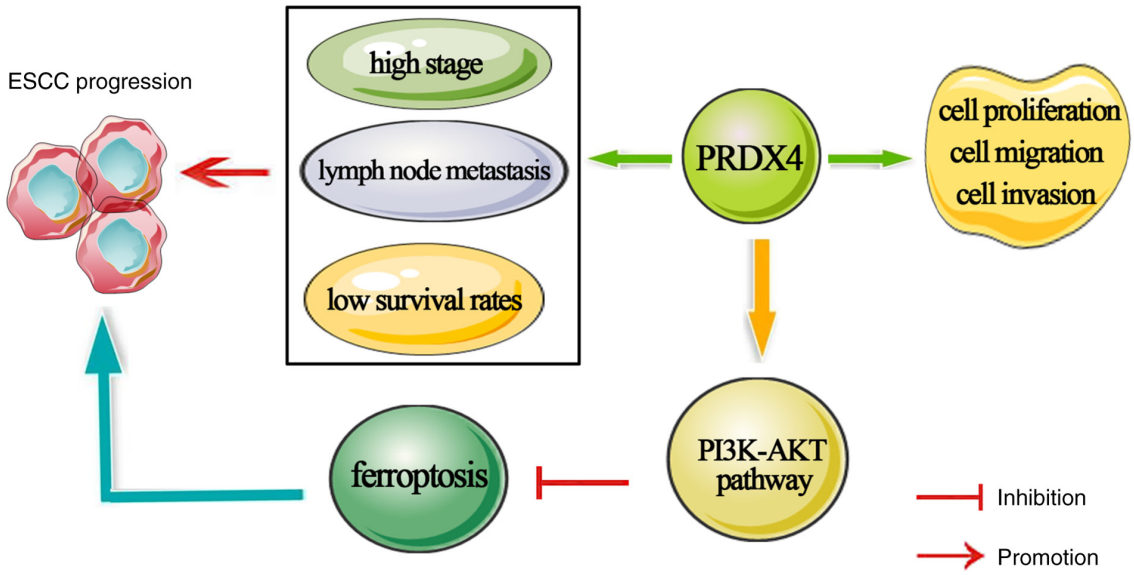

Figure 7. Proposed model of PRDX4-mediated suppression of ferroptosis through regulation of the PI3K/AKT pathway in ESCC. PRDX4 is highly expressed in ESCC samples and cells. High PRDX4 expression is strongly associated with TNM staging and lymph node metastasis in patients with ESCC and may serve as an indicator of prognosis for patients with ESCA. PRDX4 knockdown suppresses cell proliferation and invasion of ESCC cells by inactivating the PI3K/AKT signaling pathway, thereby triggering ferroptosis in these cells. PRDX4, peroxiredoxin 4; PI3K, phosphoinositide 3-kinase; AKT, protein kinase B; ESCC, esophageal squamous cell carcinoma; TNM, tumor-node-metastasis; ESCA, esophageal carcinoma.

PRDX4 suppresses ferroptosis by regulating the PI3K/AKT signaling pathway. To further elucidate the potential molecular mechanisms of PRDX4 in the regulation of ferroptosis, the effects of PRDX4 on the PI3K/AKT signaling pathway in ESCC cells were explored. It was found that the increased levels of MDA and LPO and decreased levels of GSH, upon PRDX4 depletion were partly reversed by the PI3K activator, 740 Y-P (Fig. 6A). Notably, this activator significantly reduced the levels of MDA and LPO and enhanced the levels of GSH (Fig. 6A). Further investigation revealed that PRDX4 depletion reduced the expression of GPX4, p-PI3K, and p-AKT, which was partially recovered after 740 Y-P treatment (Fig. 6B and C). Furthermore, the decrease in the levels of MDA and LPO and the increase in the levels of GSH induced by PRDX4 overexpression were significantly reversed after treatment with the PI3K inhibitor, LY294002 (Fig. 6D). Notably, LY294002 significantly increased the levels of MDA and LPO, but reduced the levels of GSH (Fig. 6D). In addition, western blotting demonstrated that PRDX4 promoted the expression of GPX4, p-PI3K, and p-AKT, and this effect was reversed when PRDX4 was overexpressed in combination with LY294002 (Fig. 6E and F). These findings indicated that PRDX4 suppresses ferroptosis by activating the PI3K/AKT signaling pathway in ESCC cells.

Discussion

The relationship between redox homeostasis and tumor development remains a hot topic of research. Therefore, targeting the genes related to redox homeostasis may provide therapeutic opportunities for various tumors. PRDX4 is an important antioxidant enzyme that widely participates in tumor progression and may be a potential prognostic biomarker for a variety of tumors (23,38,39), however, its role and molecular mechanism in the development and progression of ESCC remains unknown. The present study verified the high expression of PRDX4 in ESCC samples and cells, which was strongly linked to TNM staging and lymph node metastasis, and explained the dismal prognosis of patients with ESCA. Further investigations revealed that PRDX4 depletion suppressed ESCC cell proliferation, whereas PRDX4 overexpression had the opposite effect. Notably, PRDX4 knockdown induced ferroptosis by inhibiting the PI3K/AKT signaling pathway in ESCC cells. The findings indicated that targeting PRDX4 is a promising therapeutic approach for patients with ESCC.

Several studies have demonstrated that PRDX4 is frequently overexpressed in various tumor types. Kim *et al* (40) confirmed that PRDX4 was highly expressed in human glioblastoma cells and mouse models. Ummanni *et al* (39) found that PRDX3 and PRDX4 were overexpressed in prostate cancer samples, as was determined by reverse-phase protein arrays, and were negatively associated with TMPRSS2-ERG gene fusion (39). The iTRAQ technique revealed that PRDX4 is a metastasis-associated protein in oral squamous cell carcinoma (41). Notably, PRDX4 may be a novel prognostic marker for various tumors, including renal papillary cell carcinoma (24), colon adenocarcinoma (42), head and neck squamous cell carcinoma (43), and gastric cancer (23). These studies highlighted the clinical value of PRDX4 in most tumor types. In the present study, using bioinformatics analysis, it was found that PRDX4 is widely overexpressed in pan-cancer and ESCA, which was further validated in ESCC tissues and cells. Notably, high PRDX4 expression was strongly associated with TNM staging and lymph node metastasis in patients with ESCC. Patients with high PRDX4 expression exhibited shorter survival rates than those with low expression levels. Therefore, PRDX4 may be an important prognostic factor for patients with ESCA. The findings indicated that PRDX4 participates in the development and progression of ESCC and may be a potential prognostic factor for patients with ESCC.

Previous studies have highlighted the roles of PRDX4 in the regulation of cell proliferation, apoptosis, metastasis, and radiation resistance. Wang *et al* (17) found that PRDX4 suppressed anoikis and promoted growth and metastasis via the β-catenin/ID2 signaling pathway in hepatocellular carcinoma. In another study, PRDX4 depletion suppressed cell growth and radiation resistance, coupled with increased ROS levels, apoptosis, and DNA damage in glioblastoma cells (40). Our data also demonstrated that PRDX4 depletion suppressed cell proliferation and colony formation and reduced the number of EdU-positive cells, whereas PRDX4 overexpression promoted cell proliferation and colony formation and increased the number of EdU-positive cells in ESCC cells. In addition, the inhibition of cell migration and invasion, along with an increase of E-cadherin and a decrease in N-cadherin and vimentin expression, were observed upon PRDX4 knockdown; however, the opposite effects were observed following PRDX4 overexpression. These findings indicated that PRDX4 is a promising therapeutic target for patients with ESCC.

Ferroptosis is a cell-death pathway induced by the accumulation of phospholipid peroxides (44). GPX4 is a critical enzyme that protects cells from ferroptosis by reducing phospholipid peroxides using GSH as the reductant. Thus, GPX4 suppression can induce ferroptosis (45). SLC7A11, a key factor involved in ferroptosis, can increase intracellular cystine levels and GSH biosynthesis, thereby suppressing ferroptosis (46,47). PTGS2, an enzyme involved in lipid metabolism, promotes ferroptosis. To further explore the role of PRDX4 in ferroptosis in ESCC cells, the levels of ferroptosis-related markers were examined by western blotting. The findings revealed that PRDX4 depletion significantly increased the levels of MDA and LPO, but reduced the levels of GSH, whereas PRDX4 overexpression had the opposite effects. Stepwise investigation demonstrated that PRDX4 knockdown reduced the expression of GPX4 and SLC7A11, but enhanced the expression of PTGS2. Notably, the ferroptosis inhibitor Fer-1 partially reversed ferroptosis triggered by PRDX4 knockdown, whereas the ferroptosis inducer erastin partially promoted ferroptosis suppressed by PRDX4 overexpression in ESCC cells. Evidence suggests that PRDX4 is a major factor controlling ferroptosis in ESCC cells. The PI3K/AKT signaling pathway was shown to be critical for inhibiting ferroptosis by affecting lipid metabolism (48). The PI3K/AKT pathway was demonstrated to block ferroptosis by activating the NRF2/SLC7A11 signaling axis during cerebral ischemia (49). In the present study, it was found that the PI3K activator 740 Y-P significantly reduced the levels of MDA and LPO and increased the levels of GSH and GPX4 protein expression in ESCC cells, whereas the PI3K inhibitor LY294002 exerted the opposite effects. Notably, 740 Y-P and LY294002 partially reversed the effects of PRDX4 siRNA and PRDX4 overexpression. These findings indicated that PRDX4 suppresses ferroptosis by activating the PI3K/AKT signaling pathway. However, future studies employing genome-wide CRISPR-Cas9 screening may systematically identify PRDX4-interacting genes and novel regulatory networks involved in ferroptosis and tumor suppression. In addition, more detailed mechanistic insights require further identification of PRDX4-interacting proteins through co-immunoprecipitation coupled with mass spectrometry, which will help elucidate its functional role in ferroptosis, an aspect that will be addressed in our future studies.

In conclusion, the present study revealed that PRDX4 is highly expressed in ESCC samples and cells. High PRDX4 expression was strongly linked to TNM stage and lymph node metastasis in patients with ESCC and may be a potential prognostic indicator in patients with ESCA. PRDX4 knockdown suppressed ESCC cell proliferation and invasion by inactivating the PI3K/AKT signaling pathway, which further triggered ferroptosis in these cells (Fig. 7). These findings suggest that targeting PRDX4 is a promising therapeutic strategy for ESCC, thereby providing valuable insights into treatment approaches for patients with ESCC.

Acknowledgements

Not applicable.

Funding

The present study was supported by the Key project of Henan Provincial Science and Technology Research and Development Joint Fund (grant no. 225200810011), and Henan Province's key R&D and promotion projects (scientific and technological research) projects (grant nos. 252102311046 and 222102310099).

Availability of data and materials

The data generated in the present study may be requested from the corresponding author.

Authors' contributions

YLiu conceived and designed the current study. KL and SX performed the majority of the experiments, and interpreted the data. HL and TF performed data collection and interpretation. YLi and RR conducted the measurement of lipid peroxidation indicators, and interpreted the data. YX and SL contributed to the statistical analysis of the data. YLiu and SX wrote the original manuscript. KL and SX reviewed and revised the manuscript. KL and YLiu confirm the authenticity of all the raw data. All authors read and approved the final manuscript.

Ethical approval and consent to participate

The present study was approved (approval no. ZZUIRB 2023-239) by the Research and Ethics Committee of Zhengzhou University (Zhengzhou, China). Written informed consent was obtained from all patients.

Patient consent for publication

Not applicable.

Competing interests

The authors declare that they have no competing interests.

References

1. Bray F, Ferlay J, Soerjomataram I, Siegel RL, Torre LA and Jemal A: Global cancer statistics 2018: GLOBOCAN estimates of incidence and mortality worldwide for 36 cancers in 185 countries. CA Cancer J Clin 68: 394-424, 2018.
2. Bi B, Qiu M, Liu P, Wang Q, Wen Y, Li Y, Li B, Li Y, He Y and Zhao J: Protein post-translational modifications: A key factor in colorectal cancer resistance mechanisms. Biochim Biophys Acta Gene Regul Mech 1866: 194977, 2023.
3. Zeng H, Chen W, Zheng R, Zhang S, Ji JS, Zou X, Xia C, Sun K, Yang Z, Li H, *et al*: Changing cancer survival in China during 2003-15: A pooled analysis of 17 population-based cancer registries. Lancet Glob Health 6: e555-e567, 2018.
4. Siegel RL, Miller KD, Fuchs HE and Jemal A: Cancer statistics, 2021. CA Cancer J Clin 71: 7-33, 2021.
5. Shi Y, Fang N, Li Y, Guo Z, Jiang W, He Y, Ma Z and Chen Y: Circular RNA LPAR3 sponges microRNA-198 to facilitate esophageal cancer migration, invasion, and metastasis. Cancer Sci 111: 2824-2836, 2020.
6. Rhee SG and Kil IS: Multiple functions and regulation of mammalian peroxiredoxins. Annu Rev Biochem 86: 749-775, 2017.
7. Rhee SG: Overview on peroxiredoxin. Mol Cells 39: 1-5, 2016.
8. Fujii J, Ikeda Y, Kurahashi T and Homma T: Physiological and pathological views of peroxiredoxin 4. Free Radic Biol Med 83: 373-379, 2015.
9. Cox AG, Pearson AG, Pullar JM, Jönsson TJ, Lowther WT, Winterbourn CC and Hampton MB: Mitochondrial peroxiredoxin 3 is more resilient to hyperoxidation than cytoplasmic peroxiredoxins. Biochem J 421: 51-58, 2009.
10. Perkins A, Nelson KJ, Parsonage D, Poole LB and Karplus PA: Peroxiredoxins: Guardians against oxidative stress and modulators of peroxide signaling. Trends Biochem Sci 40: 435-445, 2015.
11. Tavender TJ and Bulleid NJ: Peroxiredoxin IV protects cells from oxidative stress by removing H2O2 produced during disulphide formation. J Cell Sci 123: 2672-2679, 2010.
12. Zito E: PRDX4, an endoplasmic reticulum-localized peroxiredoxin at the crossroads between enzymatic oxidative protein folding and nonenzymatic protein oxidation. Antioxid Redox Signal 18: 1666-1674, 2013.
13. Harris IS and DeNicola GM: The complex interplay between antioxidants and ROS in cancer. Trends Cell Biol 30: 440-451, 2020.
14. Singh A, Kukreti R, Saso L and Kukreti S: Oxidative stress: A key modulator in neurodegenerative diseases. Molecules 24: 1583, 2019.
15. Matés JM, Segura JA, Alonso FJ and Márquez J: Oxidative stress in apoptosis and cancer: An update. Arch Toxicol 86: 1649-1665, 2012.
16. Schieber M and Chandel NS: ROS function in redox signaling and oxidative stress. Curr Biol 24: R453-R462, 2014.
17. Wang W, Shen XB, Huang DB, Jia W, Liu WB and He YF: Peroxiredoxin 4 suppresses anoikis and augments growth and metastasis of hepatocellular carcinoma cells through the β-catenin/ID2 pathway. Cell Oncol (Dordr) 42: 769-781, 2019.
18. Jiang W, Wang M, Chen Q, Yu X, Liu G, He X, Mei C and Ou C: Immune infiltration related PRDX4 facilitates the malignant features and drug resistance of breast cancer. Sci Rep 15: 27507, 2025.
19. Liu Y, Han J, Shioya A, Zhang YX, Dung VA, Oyama T, Guo X, Yang Q, Ito T and Yamada S: The immunohistochemical combination of low SGLT2 expression and high PRDX4 expression independently predicts shortened survival in patients undergoing surgical resection for hepatoblastoma. Diagn Pathol 20: 2, 2025.
20. Li H, Wang Z, Chen X, Li S and Zhang F: Resveratrol downregulated PRDX4 expression to inhibit the progression of renal cell carcinoma via Wnt/β-catenin pathway. Food Sci Nutr 13: e70352, 2025.
21. Lei P, Yu L, Sun X, Hao J, Shi W, Sun H, Guo X, Jia X, Liu T, Zhang DL, *et al*: Exploring the role of PRDX4 in the development of uterine corpus endometrial carcinoma. Med Oncol 41: 48, 2024.
22. Han J, Itoh T, Shioya A, Sakurai M, Oyama T, Kumagai M, Takamura H, Okuro M, Mukai T, Kitakata H, *et al*: The combination of the low immunohistochemical expression of peroxiredoxin 4 and perilipin 2 predicts longer survival in pancreatic ductal adenocarcinoma with peroxiredoxin 4 possibly playing a main role. Histol Histopathol 38: 1415-1427, 2023.
23. Park SY, Lee YJ, Park J, Kim TH, Hong SC, Jung EJ, Ju YT, Jeong CY, Park HJ, Ko GH, *et al*: PRDX4 overexpression is associated with poor prognosis in gastric cancer. Oncol Lett 19: 3522-3530, 2020.
24. Kocatürk B: In silico analysis reveals PRDX4 as a prognostic and oncogenic marker in renal papillary cell carcinoma. Gene 859: 147201, 2023.
25. Dixon SJ, Lemberg KM, Lamprecht MR, Skouta R, Zaitsev EM, Gleason CE, Patel DN, Bauer AJ, Cantley AM, Yang WS, *et al*: Ferroptosis: An iron-dependent form of nonapoptotic cell death. Cell 149: 1060-1072, 2012.
26. Stockwell BR, Friedmann Angeli JP, Bayir H, Bush AI, Conrad M, Dixon SJ, Fulda S, Gascón S, Hatzios SK, Kagan VE, *et al*: Ferroptosis: A regulated cell death nexus linking metabolism, redox biology, and disease. Cell 171: 273-285, 2017.
27. Yang WS, SriRamaratnam R, Welsch ME, Shimada K, Skouta R, Viswanathan VS, Cheah JH, Clemons PA, Shamji AF, Clish CB, *et al*: Regulation of ferroptotic cancer cell death by GPX4. Cell 156: 317-331, 2014.
28. Bersuker K, Hendricks JM, Li Z, Magtanong L, Ford B, Tang PH, Roberts MA, Tong B, Maimone TJ, Zoncu R, *et al*: The CoQ oxidoreductase FSP1 acts parallel to GPX4 to inhibit ferroptosis. Nature 575: 688-692, 2019.
29. Mao C, Liu X, Zhang Y, Lei G, Yan Y, Lee H, Koppula P, Wu S, Zhuang L, Fang B, *et al*: DHODH-mediated ferroptosis defence is a targetable vulnerability in cancer. Nature 593: 586-590, 2021.
30. Wang SJ, Li D, Ou Y, Jiang L, Chen Y, Zhao Y and Gu W: Acetylation is crucial for p53-mediated ferroptosis and tumor suppression. Cell Rep 17: 366-373, 2016.
31. Jiang L, Kon N, Li T, Wang SJ, Su T, Hibshoosh H, Baer R and Gu W: Ferroptosis as a p53-mediated activity during tumour suppression. Nature 520: 57-62, 2015.
32. Zhao Y, Liu Z, Liu G, Zhang Y, Liu S, Gan D, Chang W, Peng X, Sung ES, Gilbert K, *et al*: Neutrophils resist ferroptosis and promote breast cancer metastasis through aconitate decarboxylase 1. Cell Metab 35: 1688-1703.e10, 2023.
33. Dos Santos AF, Fazeli G, Xavier da Silva TN and Friedmann Angeli JP: Ferroptosis: Mechanisms and implications for cancer development and therapy response. Trends Cell Biol 33: 1062-1076, 2023.
34. Torres-Velarde JM, Allen KN, Salvador-Pascual A, Leija RG, Luong D, Moreno-Santillán DD, Ensminger DC and Vázquez-Medina JP: Peroxiredoxin 6 suppresses ferroptosis in lung endothelial cells. Free Radic Biol Med 218: 82-93, 2024.
35. Fujita H, Tanaka YK, Ogata S, Suzuki N, Kuno S, Barayeu U, Akaike T, Ogra Y and Iwai K: PRDX6 augments selenium utilization to limit iron toxicity and ferroptosis. Nat Struct Mol Biol 31: 1277-1285, 2024.
36. Luo P, Liu D, Zhang Q, Yang F, Wong YK, Xia F, Zhang J, Chen J, Tian Y, Yang C, *et al*: Celastrol induces ferroptosis in activated HSCs to ameliorate hepatic fibrosis via targeting peroxiredoxins and HO-1. Acta Pharm Sin B 12: 2300-2314, 2022.
37. Livak KJ and Schmittgen TD: Analysis of relative gene expression data using real-time quantitative PCR and the 2(-Delta Delta C(T)) method. Methods 25: 402-408, 2001.
38. Guo X, Noguchi H, Ishii N, Homma T, Hamada T, Hiraki T, Zhang J, Matsuo K, Yokoyama S, Ishibashi H, *et al*: The association of peroxiredoxin 4 with the initiation and progression of hepatocellular carcinoma. Antioxid Redox Signal 30: 1271-1284, 2019.
39. Ummanni R, Barreto F, Venz S, Scharf C, Barett C, Mannsperger HA, Brase JC, Kuner R, Schlomm T, Sauter G, *et al*: Peroxiredoxins 3 and 4 are overexpressed in prostate cancer tissue and affect the proliferation of prostate cancer cells in vitro. J Proteome Res 11: 2452-2466, 2012.
40. Kim TH, Song J, Alcantara Llaguno SR, Murnan E, Liyanarachchi S, Palanichamy K, Yi JY, Viapiano MS, Nakano I, Yoon SO, *et al*: Suppression of peroxiredoxin 4 in glioblastoma cells increases apoptosis and reduces tumor growth. PLoS One 7: e42818, 2012.
41. Chang KP, Yu JS, Chien KY, Lee CW, Liang Y, Liao CT, Yen TC, Lee LY, Huang LL, Liu SC, *et al*: Identification of PRDX4 and P4HA2 as metastasis-associated proteins in oral cavity squamous cell carcinoma by comparative tissue proteomics of microdissected specimens using iTRAQ technology. J Proteome Res 10: 4935-4947, 2011.
42. Zhou H, Li L, Chen J, Hou S, Zhou T and Xiong Y: Expression and prognostic value of PRDX family in colon adenocarcinoma by integrating comprehensive analysis and in vitro and in vivo validation. Front Oncol 13: 1136738, 2023.

43. Cao R, Zhang W, Zhang H, Wang L, Chen X, Ren X, Cheng B and Xia J: Comprehensive analysis of the PRDXs family in head and neck squamous cell carcinoma. Front Oncol 12: 798483, 2022.
44. Jiang X, Stockwell BR and Conrad M: Ferroptosis: Mechanisms, biology and role in disease. Nat Rev Mol Cell Biol 22: 266-282, 2021.
45. Stockwell BR: Ferroptosis turns 10: Emerging mechanisms, physiological functions, and therapeutic applications. Cell 185: 2401-2421, 2022.
46. Guo W, Zhao Y, Zhang Z, Tan N, Zhao F, Ge C, Liang L, Jia D, Chen T, Yao M, *et al*: Disruption of xCT inhibits cell growth via the ROS/autophagy pathway in hepatocellular carcinoma. Cancer Lett 312: 55-61, 2011.
47. Huang Y, Dai Z, Barbacioru C and Sadée W: Cystine-glutamate transporter SLC7A11 in cancer chemosensitivity and chemoresistance. Cancer Res 65: 7446-7454, 2005.
48. Xu J, Li Y, Kang M, Chang C, Wei H, Zhang C and Chen Y: Multiple forms of cell death: A focus on the PI3K/AKT pathway. J Cell Physiol 238: 2026-2038, 2023.
49. Fu C, Wu Y, Liu S, Luo C, Lu Y, Liu M, Wang L, Zhang Y and Liu X: Rehmannioside A improves cognitive impairment and alleviates ferroptosis via activating PI3K/AKT/Nrf2 and SLC7A11/GPX4 signaling pathway after ischemia. J Ethnopharmacol 289: 115021, 2022.